SANDIA REPORT
SAND2014-2373
Unlimited Release
Printed March, 2014

A Method for the Quantification of Model Form Error Associated with Physical Systems

Samuel P. Wallen and Matthew R. Brake

Prepared by
Sandia National Laboratories
Albuquerque, New Mexico 87185 and Livermore, California 94550

Sandia National Laboratories is a multi-program laboratory managed and operated by Sandia Corporation, a wholly owned subsidiary of Lockheed Martin Corporation, for the U.S. Department of Energy's National Nuclear Security Administration under contract DE-AC04-94AL85000.

Approved for public release; further dissemination unlimited.

Sandia National Laboratories

Issued by Sandia National Laboratories, operated for the United States Department of Energy by Sandia Corporation.

NOTICE: This report was prepared as an account of work sponsored by an agency of the United States Government. Neither the United States Government, nor any agency thereof, nor any of their employees, nor any of their contractors, subcontractors, or their employees, make any warranty, express or implied, or assume any legal liability or responsibility for the accuracy, completeness, or usefulness of any information, apparatus, product, or process disclosed, or represent that its use would not infringe privately owned rights. Reference herein to any specific commercial product, process, or service by trade name, trademark, manufacturer, or otherwise, does not necessarily constitute or imply its endorsement, recommendation, or favoring by the United States Government, any agency thereof, or any of their contractors or subcontractors. The views and opinions expressed herein do not necessarily state or reflect those of the United States Government, any agency thereof, or any of their contractors.

Printed in the United States of America. This report has been reproduced directly from the best available copy.

Available to DOE and DOE contractors from
U.S. Department of Energy
Office of Scientific and Technical Information
P.O. Box 62
Oak Ridge, TN 37831

Telephone: (865) 576-8401
Facsimile: (865) 576-5728
E-Mail: reports@adonis.osti.gov
Online ordering: http://www.osti.gov/bridge

Available to the public from
U.S. Department of Commerce
National Technical Information Service
5285 Port Royal Rd.
Springfield, VA 22161

Telephone: (800) 553-6847
Facsimile: (703) 605-6900
E-Mail: orders@ntis.fedworld.gov
Online order: http://www.ntis.gov/help/ordermethods.asp?loc=7-4-0#online

SAND2014-2373
Unlimited Release
Printed March 2014

A Method for the Quantification of Model Form Error Associated with Physical Systems

Samuel P. Wallen and Matthew R. Brake
Component Science and Mechanics
Sandia National Laboratories
P.O. Box 5800
Albuquerque, New Mexico 87185-MS1070

Abstract

In the process of model validation, models are often declared valid when the differences between model predictions and experimental data sets are satisfactorily small. However, little consideration is given to the effectiveness of a model using parameters that deviate slightly from those that were fitted to data, such as a higher load level. Furthermore, few means exist to compare and choose between two or more models that reproduce data equally well. These issues can be addressed by analyzing model form error, which is the error associated with the differences between the physical phenomena captured by models and that of the real system. This report presents a new quantitative method for model form error analysis and applies it to data taken from experiments on tape joint bending vibrations. Two models for the tape joint system are compared, and suggestions for future improvements to the method are given. As the available data set is too small to draw any statistical conclusions, the focus of this paper is the development of a methodology that can be applied to general problems.

ACKNOWLEDGMENTS

The authors thank Daniel Segalman for his assistance in developing the calculation methods used in this report. The authors also thank Mike Starr and Dan Segalman for their permission to use data from SAND2012-6527 and for their assistance in interpreting it.

CONTENTS

A Method for the Quantification of Model Form Error Associated with Physical Systems 3

Acknowledgments 4

Figures 6

Tables 7

Nomenclature 8

1. Introduction 9

2. Calculation of Model Form Error 11
   2.1. Fundamental Quantities 11
   2.2. Model Form Error 11
   2.3. Model Form Error from a Distribution 12
   2.4. Model Form Error Average 12

3. Application to Tape Joint Bending Vibrations 15
   3.1. Overview of Tape Joints 15
   3.2. Linear Oscillator Model Results 16
   3.3. Duffing Oscillator Model Results 18
   3.4. Comparison of Linear and Duffing Models 20
      3.4.1. Other Models to Consider 23

4. Future Work 25
   4.1. Bandwidth Selection 25
   4.2. Sampling from a Distribution 25
      4.2.1. Finding Samples 25
      4.2.2. Problems with this Method 26

5. Conclusions 27

Appendix A: Equations for Linear Oscillator Model 29
   Model and Inverse Model Functions 30
   Summary 31

Appendix B: Equations for Duffing Oscillator Model 33
   Model and Inverse Model Functions 35
      Using Analytical Approximations 35
      Using Numerical Continuation 36
   Summary 37

Appendix C: Duffing Model with Amplitude-Affected Damping 39

Appendix D: One-Way Compliant Duffing Oscillator Model 43

Appendix E: Kernel Density Estimation 45

Appendix F: Numerical Continuation Method 47

References 49

Distribution 51

FIGURES

Figure 1: Schematics of a tape joint, and photo of an assembly containing a tape joint. 15
Figure 2: Acceleration FRF plot of a tape joint specimen undergoing bending vibrations. The force amplitudes are 1 lb (blue), 5 lb (green), and 10 lb (red). Solid lines are associated with tests employing downward sweeps in excitation frequency, and dashed lines are associated with upward sweeps in excitation frequency. Courtesy of Dan Segalman and Michael Starr [5]..... 16
Figure 3: Histograms of the resonant frequency MFE and resonant amplitude MFE for the linear model..... 17
Figure 4: Histograms of the resonant frequency MFED and resonant amplitude MFED for the linear model. 18
Figure 5: Histograms of the jump-down frequency MFE, jump-down amplitude MFE, jump-up frequency MFE, and jump-up amplitude MFE for the Duffing model..... 19
Figure 6: Histograms of the jump-down frequency MFED, jump-down amplitude MFED, jump-up frequency MFED, and jump-up amplitude MFED for the Duffing model..... 20
Figure 7: MFED of the linear model with the Duffing model features of interest. 21
Figure 8: MFEA of the linear model..... 22
Figure 9: MFEA of the Duffing model. 22
Figure 10. Schematic of Linear Oscillator Model 29
Figure 11: FRF of a linear oscillator in terms of the amplitude, real part of the stability variable (where values greater than 0 indicate unstable responses), and imaginary part of the stability variable..... 30
Figure 12. Schematic of Duffing Oscillator Model 33
Figure 13: FRF of a linear oscillator in terms of the amplitude, real part of the stability variable (where values greater than 0 indicate unstable responses), and imaginary part of the stability variable. Blue points in the amplitude plot represent stable responses, and red points represent unstable responses..... 34
Figure 14. FRF of a Duffing oscillator with amplitude-affected damping in terms of the amplitude, real part of the stability variable (where values greater than 0 indicate unstable responses), and imaginary part of the stability variable. Blue points in the amplitude plot represent stable responses, and red points represent unstable responses..... 40
Figure 15. FRF of a DMAAD with negative overall damping with amplitude-affected damping in terms of the amplitude, real part of the stability variable (where values greater than 0 indicate unstable responses), and imaginary part of the stability variable. Blue points in the amplitude plot represent stable responses, and red points represent unstable responses..... 41
Figure 16. FRF of a one-way compliant duffing oscillator with amplitude-affected damping in terms of the amplitude, real part of the stability variable (where values greater than 0 indicate unstable responses), and imaginary part of the stability variable. Blue points in the amplitude plot represent stable responses, and red points represent unstable responses..... 44
Figure 17. Example of Duffing Oscillator FRF with Features of Interest..... 48

TABLES

Table 1: Definition of fundamental quantities 11
Table 2: KDE bandwidths and number of samples for the linear model. 17
Table 3. KDE bandwidths and number of samples for the Duffing model. 19
Table 4. Summary of Linear Oscillator Model 31
Table 5. Summary of Duffing Oscillator Model 37

NOMENCLATURE

DMAAD	Duffing Model with Amplitude Affected Damping
DOF	Degree(s) of Freedom
FRF	Frequency Response Function
KDE	Kernel Density Estimator
MFE	Model Form Error
MFEA	Average Model Form Error
MFED	Model Form Error from Distribution
PDF	Probability Density Function
RMS	Root-Mean-Square

1. INTRODUCTION

Model validation is the process of determining the degree to which a model is an accurate representation of the real world from the perspective of the intended uses of the model. For physical systems, this is usually accomplished by comparing a set of model predictions to a set of experimental results and refining the model until the two data sets are in satisfactory agreement. However, the following problems may arise:

1. The error between the model predictions and the experimental data may be very sensitive to small variations in model parameters.
2. It may be possible to find many models, each accounting for different physics, that appear to fit the range of experimental data equally well.

Each of these problems appears because the physical phenomena taken into account by the models may not actually reflect the physics of the real system. The discrepancy between modeled physics and the true physics of the system is called model form error (MFE). In order for a particular model to be properly validated and be the most appropriate model, its MFE should be at a minimum.

Currently, there are no widely accepted methods that can be used to quantify MFE while addressing the problems mentioned above. Akaike's entropy-based information criterion [1] is a method that is widely used throughout many different research fields, including economics, psychometrics, ecology, and medicine. This report proposes a new extension of Akaike's entropy-based information criterion to calculate MFE based on the concept of minimizing information entropy [2, 3, 4] and use it to assess the validity of models representing physical systems. The concept of minimizing information entropy in order to select the most appropriate physical model for an engineering system was first proposed in [5], and is summarized as selecting the model that exhibits the lowest amount of parameter variation in fitting a set of data. For instance, if two models are used to fit a set of data for a single system resulting in one model having parameters that vary significantly while the other model has parameters that vary by only a few percent, the model with the larger variation in fitted parameters is said to have a higher information entropy. By minimizing the information entropy, it is hypothesized that the resulting model is more representative of the real system since the real system's parameters should not be changing appreciably as a model with high information entropy would imply.

As Akaike's entropy-based information criterion is a widely adopted method in several branches of statistics, there have been numerous extensions and refinements of the method [6]. These extensions have developed metrics to assess the complexity of a model [7] since a very complex model can fit the data well without necessarily having any interpretable relationship with the physical phenomena [8]. The use of information entropy is further extended to calculating a fuzzy distribution of the inputs for different models from the fuzzy distribution of measured outputs [9]. Once the inputs are identified, the model that predicts the correct response space with the least aleatoric uncertainty in input parameters is identified as the optimal model to use.

Other alternatives to Akaike's information criterion, of course, exist [10]. One recent method is to use polynomial chaos to assess epistemic uncertainty when incomplete or approximate

distributions of parameters exist [11, 12], or when data is convoluted with aleatoric uncertainty [13]. The maximum likelihood estimation method is another approach, developed in parallel to Akaike's information criterion, that deduces model parameters and statistical reliability from discrete time series [14, 15, 16].

In the following sections, the process for calculating MFE is presented, and the method is used to compare two models for bending vibrations in a tape joint (one linear model and one nonlinear model). This report concludes with suggestions for future improvements of the MFE calculation method.

It should be noted that the intended purpose of this report is to introduce a new methodology for MFE quantification. The available data set for the tape joint application is far too small for use in a real model validation, and the results presented here are only meant to illustrate an example application of this methodology. While the results given are not intended to validate or invalidate any particular model, the authors hope that the methodology presented here will eventually be used in applications where larger, more reasonable amounts of data are available.

2. CALCULATION OF MODEL FORM ERROR

The processes for calculating the various types of MFE are outlined below.

2.1. Fundamental Quantities

In order to calculate MFE, the following quantities must be defined:

Table 1: Definition of fundamental quantities

Variable	Definition
α_n^j	The nth parameter of fit for a model with N fitted parameters, fitted using the jth data point.
p_i^j	The ith feature of interest predicted by a model fitted using the jth data point.
x_i^j	The ith feature of interest taken from the jth data point of a set of experimental data
α^j	A vector containing all N elements of α_n^j.
p^j	A vector containing all I elements of p_n^j.
x^j	A vector containing all I elements of x_n^j.
I	The number of different features of interest.
N	The number of fitted parameters.
$M(\alpha^j)$	The model that maps the fitted parameters α^j onto the predicted features of interest p, such that $M(\alpha^j) = p^j$.
$M^{-1}(x^j)$	The inverse model of M that maps the experimental features of interest x^j onto the fitted parameters α^j for the jth data point, such that $M^{-1}(x^j) = \alpha^j$.

Note that x and p must represent the same quantity in order to be compared, but x need not be the raw experimental data itself; it can be calculated later.

2.2. Model Form Error

The model form error for a particular model M and experimental data set x is defined by the following two-dimensional array:

$$MFE_i^k(M,x) \equiv \sqrt{\frac{1}{J}\sum_{j=1}^{J}\left(\frac{p_i^k - x_i^j}{x_i^j}\right)^2} \equiv \sqrt{\frac{1}{J}\sum_{j=1}^{J}\left(\frac{M\left(M^{-1}(x^k)\right) - x_i^j}{x_i^j}\right)^2}$$

The superscripted indices represent the J data points, and the subscripted index represents the I features of interest. Here, two superscripted indices are used because the model predictions

calculated for each data point are compared with all data points; therefore, MFE_i^k has IJ elements. Each element is the RMS error of the ith feature of interest predicted using the kth data point, where the mean under the square root is computed over the J data points.

2.3. Model Form Error from a Distribution

More generally, α_n can be sampled many times from N probability density functions derived from the experimental data using kernel density estimation. The kernel density estimation process is detailed in Appendix E:. In this case, the MFE must be calculated for every combination of sampled parameters. Therefore, the model form error for a distribution of fitted parameters is defined by

$$MFED_i^\eta(M,x) \equiv \sqrt{\frac{1}{J}\sum_{j=1}^{J}\left(\frac{p_i^\eta - x_i^j}{x_i^j}\right)^2} \equiv \sqrt{\frac{1}{J}\sum_{j=1}^{J}\left(\frac{M(\alpha^\eta) - x_i^j}{x_i^j}\right)^2}$$

where η represents N different indices, one for each fitted parameter. Each of these N indices takes on integer values from one to the number of samples collected for its respective parameter. Therefore, $MFED_i^\eta$ has a number of elements equal to

$$I\prod_{n=1}^{N} S_n$$

where S_n is the number of samples of the nth fitted parameter.

After MFE_i^k and $MFED_i^\eta$ are calculated, they are displayed as I histograms. Each histogram represents the MFE of a particular feature of interest for a particular model and experimental data set.

2.4. Model Form Error Average

In order to compare the MFEs from distributions of two or more models, a normalized average error taken over all features of interest must be defined:

$$MFEA^\eta = \frac{1}{I}\sum_{i=1}^{I} MFED_i^\eta$$

Thus two models may be compared as long as the same features of interest can be calculated from each.

In the results for the tape joint bending vibration problem presented later, the MFE of a model will refer to the model form error based on models fitted directly from the data (MFE_i^k above), the $MFED$ of a model will refer to the model form error based on models with parameters sampled from a distribution that resembles the data ($MFED_i^\eta$ above), and the $MFEA$ of a model will refer to the average error over all features of interest ($MFEA^\eta$ above).

3. APPLICATION TO TAPE JOINT BENDING VIBRATIONS

3.1. Overview of Tape Joints

A tape joint is a joining method used to connect two cylinders in an end-to-end manner, as shown in Figure 1. The appeal of tape joints is due to their high strength, low weight, ease of assembly, and ability to provide a smooth exterior surface.

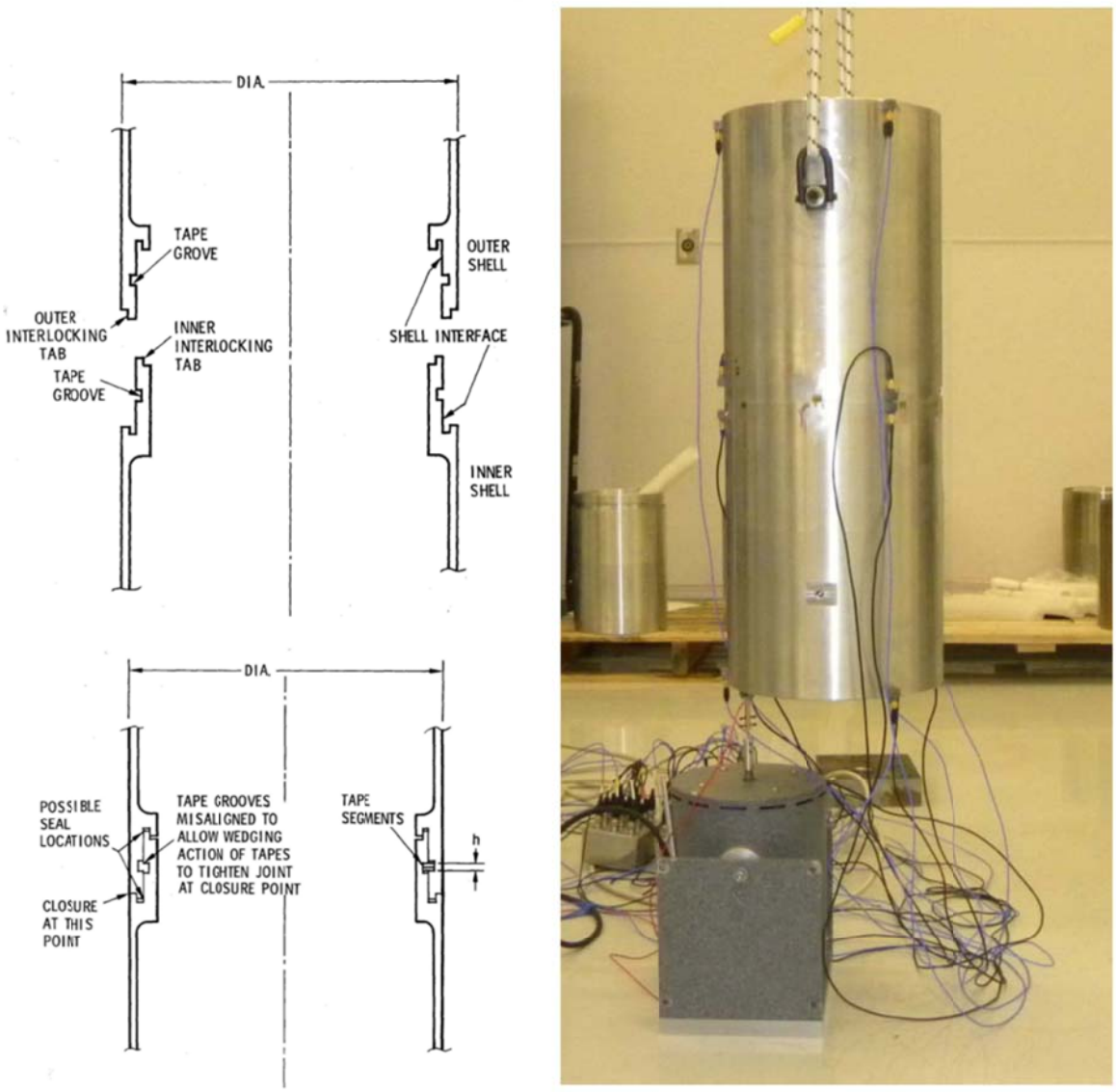

Figure 1: Schematics of a tape joint, and photo of an assembly containing a tape joint.

Experimental results presented in [17] showed that the dynamics of bending vibrations in tape joints are nonlinear. As the bending amplitude increases, the point of closure of the joint tends to open; this causes a reduction in the effective stiffness of the joint. An FRF plot of acceleration for a tape joint specimen undergoing bending vibrations is reproduced from [17] in Figure 2.

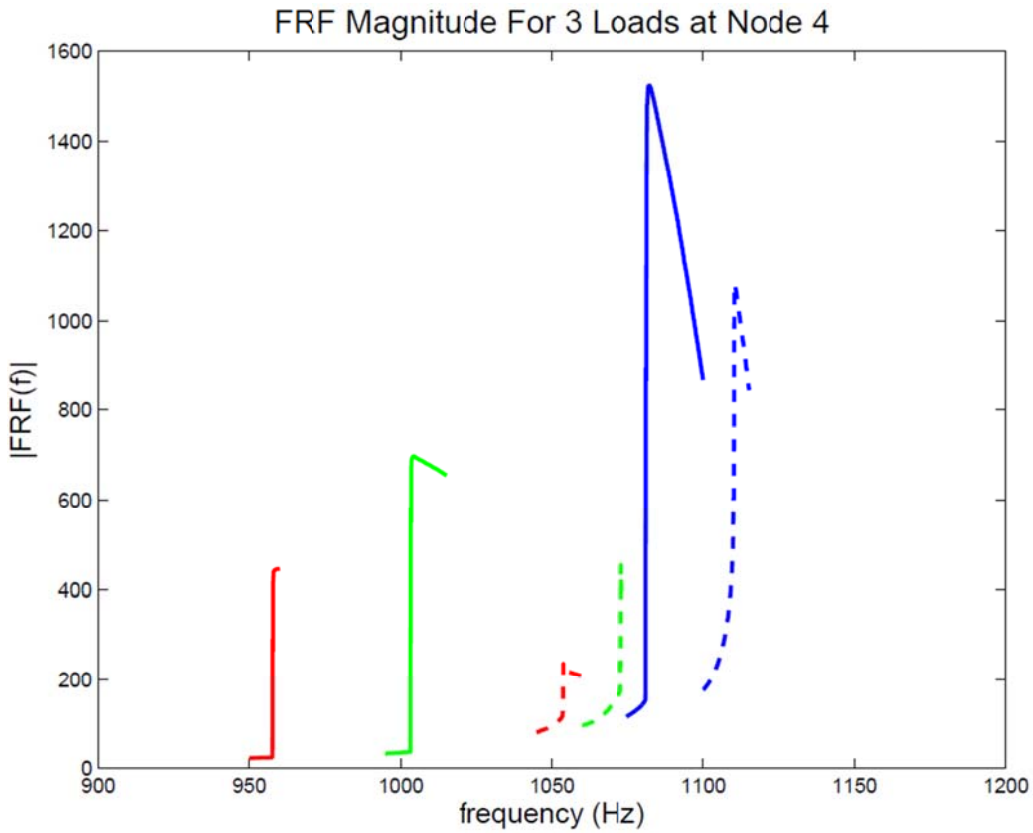

Figure 2: Acceleration FRF plot of a tape joint specimen undergoing bending vibrations. The force amplitudes are 1 lb (blue), 5 lb (green), and 10 lb (red). Solid lines are associated with tests employing downward sweeps in excitation frequency, and dashed lines are associated with upward sweeps in excitation frequency. Courtesy of Dan Segalman and Michael Starr [17].

Two models are fitted to the FRF data of Figure 2. The first model is a simple linear oscillator, and the second model is a Duffing oscillator (a nonlinear oscillator with a cubically-varying stiffness). MFEs and MFEDs are calculated for each model, and the results are presented in the following two subsections.

3.2. Linear Oscillator Model Results

The first model used to fit the tape joint FRF data was a single-degree-of-freedom oscillator with linear stiffness and damping. Since there are six peaks in the FRF plot, six data points are used. The frequency and amplitude of each peak (features of interest) are used to calculate the natural frequency and damping ratio (fitted parameters) of the model. A detailed description of the linear model is presented in Appendix A:. The MFE of the linear model is shown as a histogram in Figure 3.

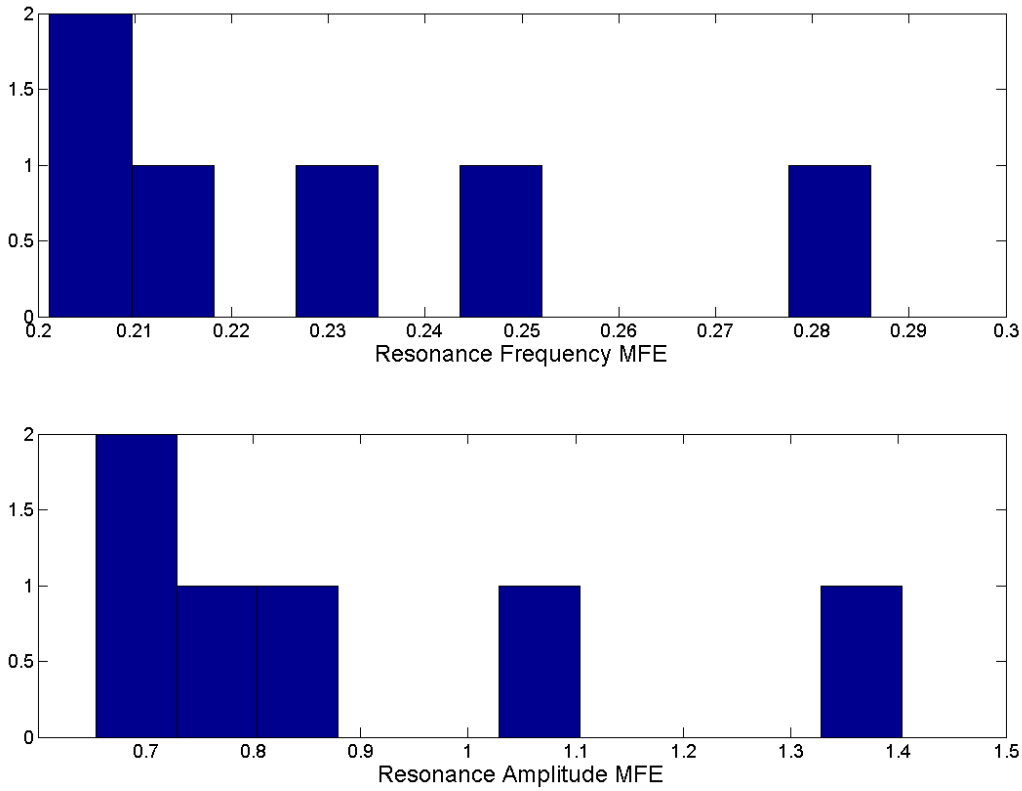

Figure 3: Histograms of the resonant frequency MFE and resonant amplitude MFE for the linear model.

PDFs of the model natural frequency and damping ratio are generated using kernel density estimation. These model parameters are sampled from the PDFs, and the MFED of the linear model is calculated. The bandwidths of the kernel density estimators and the numbers of samples for the parameters are shown below in Table 2, and the MFED histograms are shown in Figure 4.

Table 2: KDE bandwidths and number of samples for the linear model.

Model Parameter	***KDE Bandwidth***	***Number of Samples***
Natural Frequency	50	100
Damping Ratio	0.0002	100

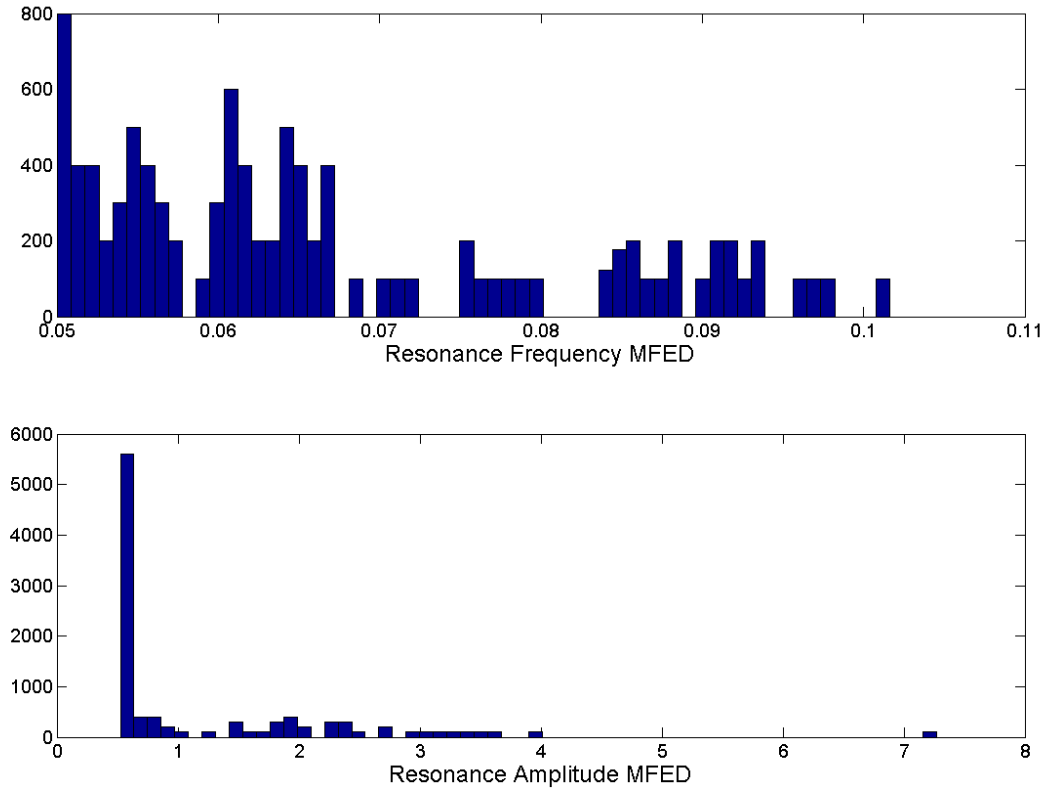

Figure 4: Histograms of the resonant frequency MFED and resonant amplitude MFED for the linear model.

3.3. Duffing Oscillator Model Results

The second model used to fit the tape joint FRF data is a single-degree-of-freedom Duffing oscillator. The Duffing oscillator has linear stiffness and damping, but has an additional nonlinear stiffness parameter. When normalized in the same manner as in [18], the Duffing model has four features of interest (jump-down frequency, jump-down amplitude, jump-up frequency, and jump-up amplitude), and two fitted parameters (nonlinearity parameter and damping ratio). The tape joint FRF data contains curves for three loading conditions, each having the four features of interest; therefore, three data points are available for use with the Duffing model. A detailed description of the Duffing model is presented in Appendix B:.

The results that follow are obtained using the numerical continuation method described in Appendix B:. The continuation method is more accurate than the analytical approximation method, but has a much longer computational time.

The MFE for the Duffing model is shown as a histogram in Figure 5. Note that only three data points are available for this particular analysis; in the case of a real model validation, many more data points would be necessary.

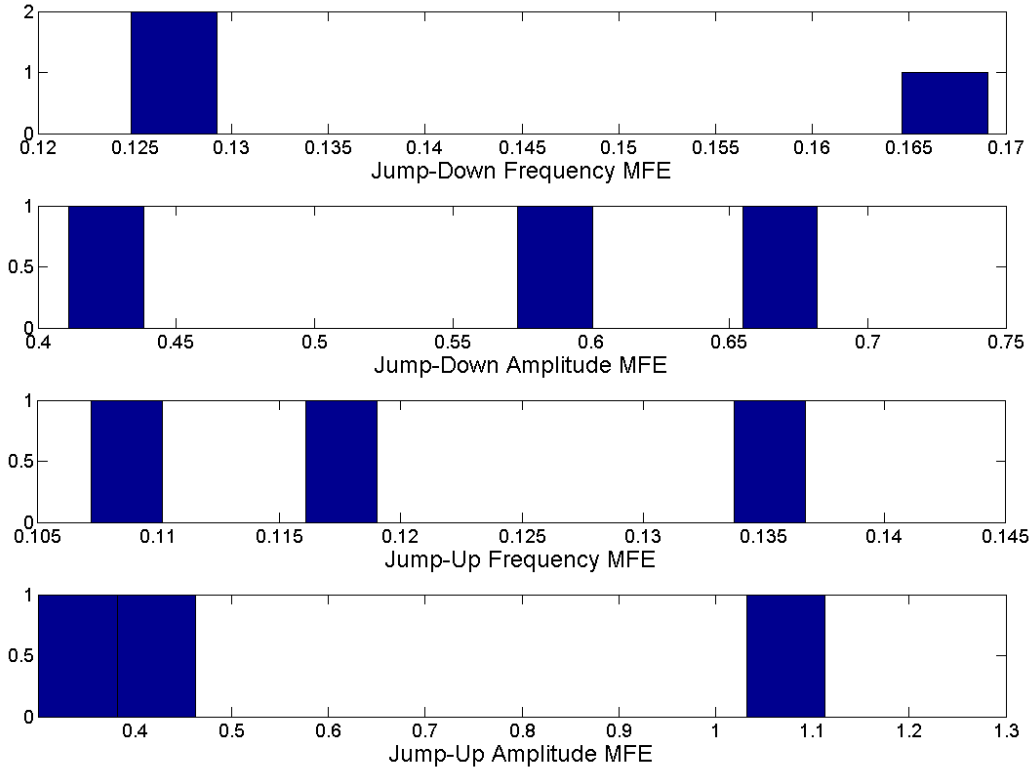

Figure 5: Histograms of the jump-down frequency MFE, jump-down amplitude MFE, jump-up frequency MFE, and jump-up amplitude MFE for the Duffing model.

In the same way as is done for the linear model, PDFs of the nonlinearity parameter and damping parameter were generated using kernel density estimation. These model parameters are sampled from the PDFs, and the MFED of the Duffing model iss calculated. The bandwidths of the kernel density estimators and the numbers of samples for the parameters are shown below in Table 3, and the MFED histograms are shown in Figure 6.

Table 3. KDE bandwidths and number of samples for the Duffing model.

Model Parameter	***KDE Bandwidth***	***Number of Samples***
Nonlinearity Parameter	$1 \text{ X } 10^{-6}$	50
Damping Parameter	0.003	50

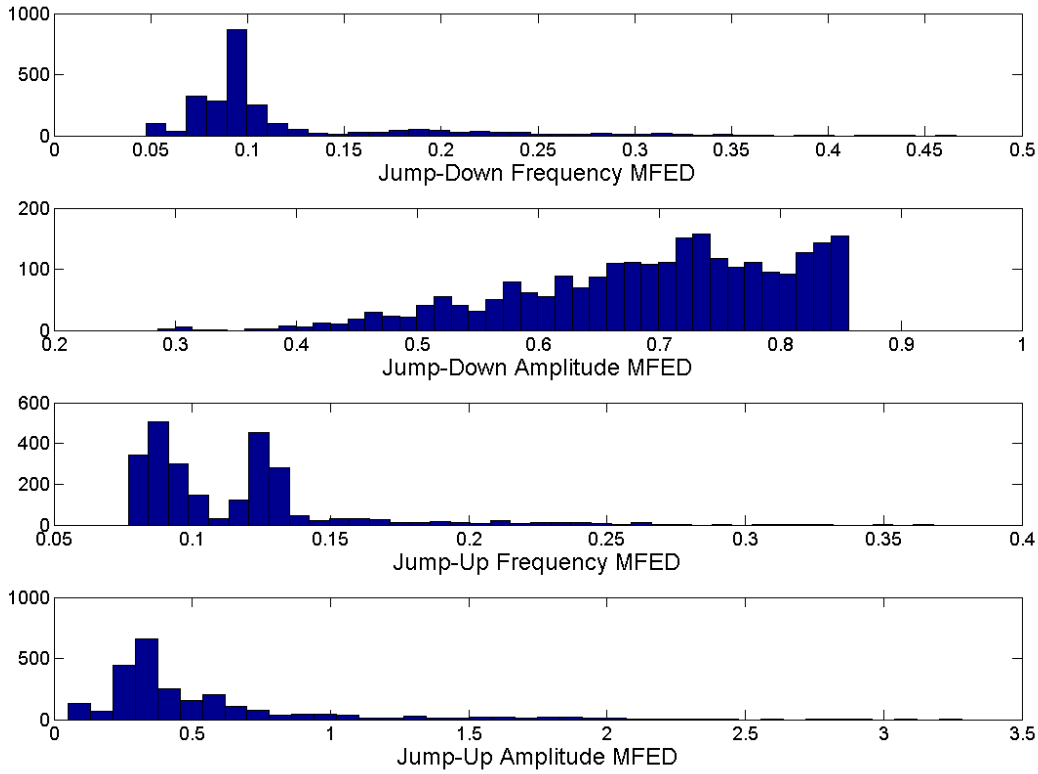

Figure 6: Histograms of the jump-down frequency MFED, jump-down amplitude MFED, jump-up frequency MFED, and jump-up amplitude MFED for the Duffing model.

3.4. Comparison of Linear and Duffing Models

In order to compare the two models, the MFED of the linear model had to be recalculated to match the features of interest of the Duffing model; that is, for each set of sampled linear model parameters, the resulting predicted features of interest had to be compared separately to the jump-up and jump-down features of the Duffing model. The MFED of the linear model (with the features of interest of the Duffing model) is shown in Figure 7.

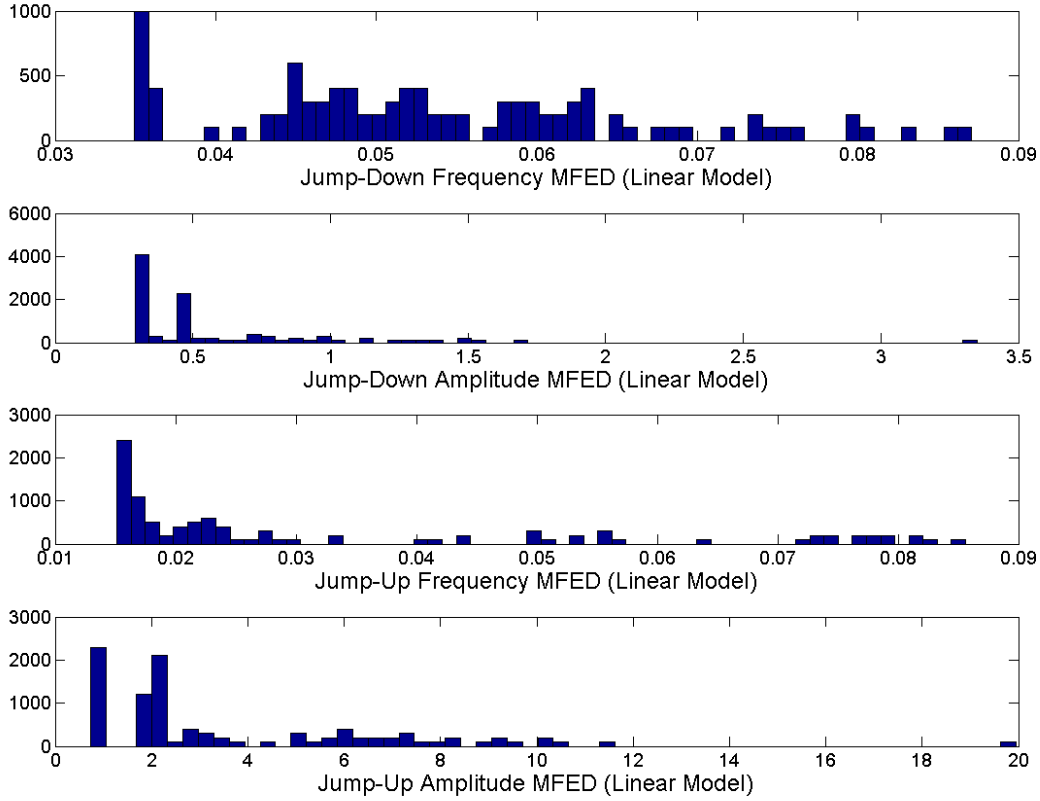

Figure 7: MFED of the linear model with the Duffing model features of interest.

The MFEA of each model is calculated by finding the mean of each MFED across all features of interest. The MFEAs of the linear and Duffing models are shown in Figure 8 and Figure 9, respectively.

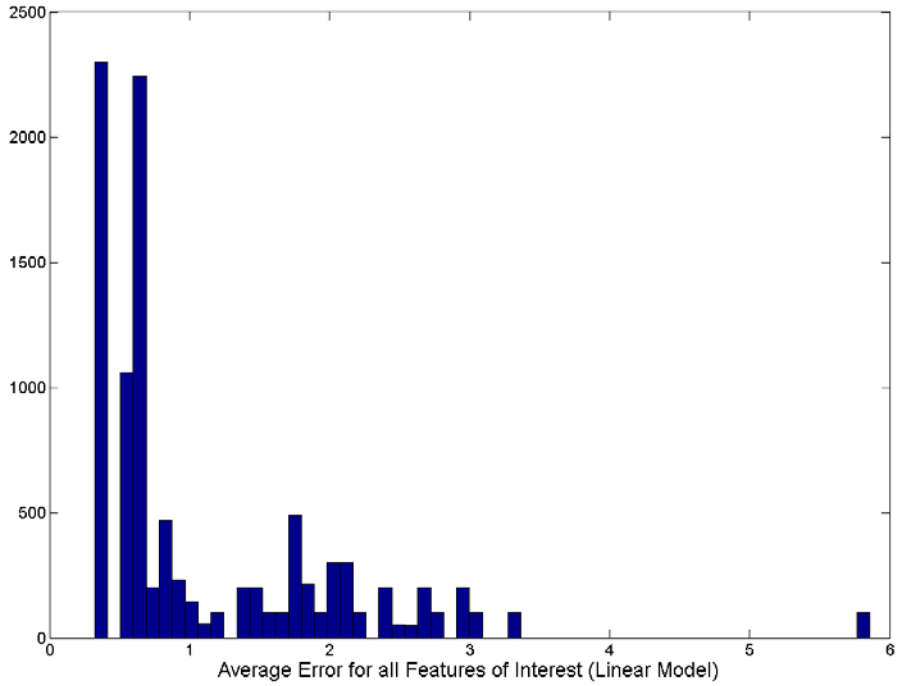

Figure 8: MFEA of the linear model.

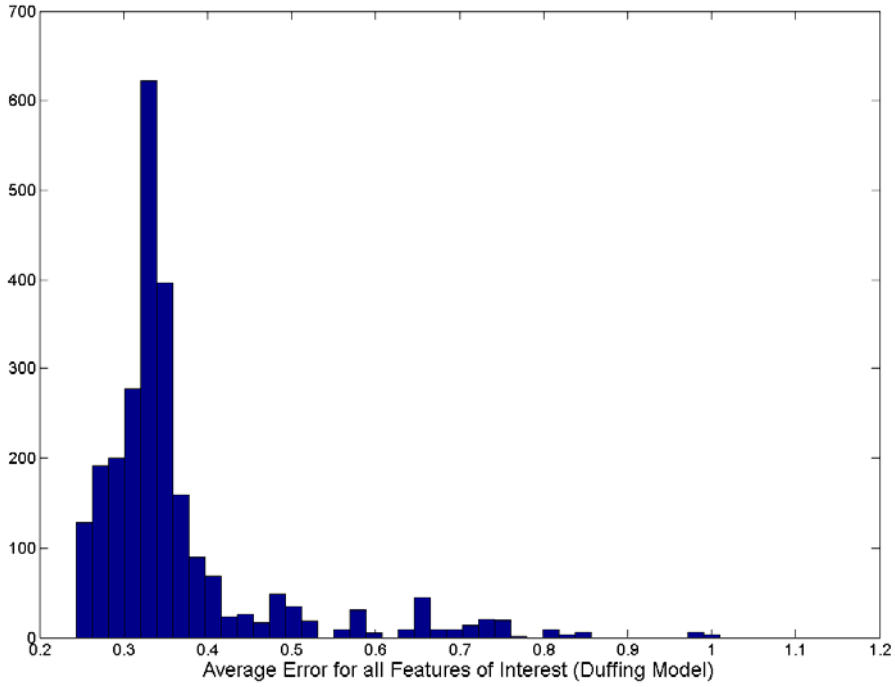

Figure 9: MFEA of the Duffing model.

As shown in Figure 8 and Figure 9, the MFEA of the linear model (ranging from approximately 30% to 600%) is much greater than that of the Duffing model (ranging from approximately 25% to 100%, with most values between 25% and 40%). This result makes sense because the linear model has only one characteristic frequency and one characteristic amplitude that can be compared to the data, but the data clearly has two characteristic frequencies and two amplitudes per point. Because the Duffing model naturally can accommodate all four features of interest present in the data, it has a much lower MFEA.

3.4.1. Other Models to Consider

While the MFEA of the Duffing model is generally much lower than that of the linear model, it still has more than 20% average error for all sampled parameter combinations. This implies that it may be possible to find a model that fits the tape joint data with much less error.

One suggested model to examine in future work is

$$m\ddot{x} + (c_1 + c_2 x^2)\dot{x} + k_1 x + k_3 x^3 = A\sin(\omega t)\ .$$

This equation is similar to that of the Duffing oscillator, but has an additional term that allows the overall damping of the system to vary with the response amplitude. According to [17], the nonlinearity in the FRF of the tape joint structure is thought to exist because some regions of the joined surfaces lose contact at high amplitudes of vibration; this produces the *softening* (reduction if stiffness) effect shown in the FRF data. Using this proposed model, a reduction in damping at high amplitudes can also be accommodated by setting $c_2 < 0$. More detail about this model is given in Appendix C:.

Another model to consider is the one-way compliant Duffing oscillator, given by

$$m\ddot{x} + c\dot{x} + k_1 x + k_3(x) * x^3 = A\sin(\omega t)$$

$$k_3(x) = \begin{cases} K_3, & x > 0 \\ 0, & x \leq 0 \end{cases}\ .$$

This model is also similar to the ordinary Duffing oscillator; the only difference is that the nonlinear stiffness term is non-zero only when $x > 0$. More detail about this model is given in Appendix D:.

4. FUTURE WORK

The following subsections provide recommendations for improvements to be made to the MFE calculation process in the future.

4.1. Bandwidth Selection

If the MFEDs of two models describing a single physical system are calculated using KDEs with drastically different smoothness, it would not be reasonable to compare the two models on the basis of MFED. This is because a KDE with a higher smoothness would allow much more variation in the sampling of model parameters for a single model, resulting in dramatic changes in the MFED. Therefore, in order to make a fair comparison between the MFEDs of two or more models for a single physical system, the bandwidths of the KDEs used to sample the fitted model parameters should be chosen such that the KDEs are all of similar smoothness.

While the smoothness of a KDE can be approximately determined by visual inspection of its plot, it is recommended that a systematic method for bandwidth selection be developed. This would allow fairer comparisons between models on the basis of their MFEDs.

4.2. Sampling from a Distribution

When calculating MFED, a large number of model parameter values must be sampled from the distributions described by the KDEs. While this process is simple in concept, there are some problems that arise in implementation.

4.2.1. Finding Samples

Currently, the fitted model parameters used in the calculation of MFED are sampled from the distributions defined by the KDEs using the following process:

The cumulative probability density function KDEC of each KDE is found by computing

$$KDEC(x) \approx \int_{\mu-n\sigma}^{x} KDE(x)\,dx\,,$$

where μ is the mean of the model parameters taken directly from experimental data, σ is the standard deviation, and n is a positive integer that can be adjusted. This integral is calculated numerically, with the highest value of x usually being $\mu + n\sigma$. The positive integer n should be chosen so that the integral is a satisfactory approximation of

$$\int_{-\infty}^{\infty} KDE(x)\,dx\,,$$

which is the true cumulative density function. That is, n should be chosen such that

$$KDEC(\mu - n\sigma) \approx 0$$

and

$$KDEC(\mu + n\sigma) \approx 1\ .$$

A random number generator is used to generate S numbers between 0 and 1, where S is the number of samples desired for the model parameter.

Treating $KDEC(x)$ as the independent variable and model parameter values x as the dependent variable, interpolation is used to find the values of x corresponding to $KDEC(x)$ evaluated at the random numbers generated in the previous step. The interpolated values of x are the S samples of the model parameter.

4.2.2. Problems with this Method

Depending on the shape of $KDE(x)$, $KDEC(x)$ may be difficult to compute accurately. For example, the numerically computed vector of values describing $KDEC(x)$ could jump up discontinuously from the first element, which is 0, to the second element. This vector could also reach a value of 1 (within numerical precision) before the last element and remain at that value, which causes problems with the interpolation process (the interpolation function used in the tape joint application above requires the independent variable to increase monotonically).

While there are some ways to work around these problems (increasing the value of n can sometimes help, for example), it would be beneficial to find a more sophisticated and more accurate way to find samples from a distribution. This would ensure that the samples resemble their respective KDEs as closely as possible.

5. CONCLUSIONS

In this work, a method for the quantification of model form error is developed and applied to data taken from experiments on tape joined structures. As expected, the average error of the linear model is significantly greater than that of the Duffing model; this is due to the fact that the linear model has fewer characteristic frequencies and amplitudes than the data appeared to contain. However, it is important to note that the data set used here is too small to convincingly validate or invalidate either model. Consequently, the present work is focused on developing a methodology that can be applied to a larger data set once it becomes available.

With the improvements discussed in the previous section, the authors hope that the methods of model form error analysis presented here will become a useful aid in the process of model validation and uncertainty quantification.

APPENDIX A: EQUATIONS FOR LINEAR OSCILLATOR MODEL

A diagram of the system described by the single-DOF linear oscillator model is shown in Figure 10, where m, c, and k are the lumped mass, damping, and stiffness of the system, respectively, and A is the amplitude of a sinusoidal load with angular frequency ω.

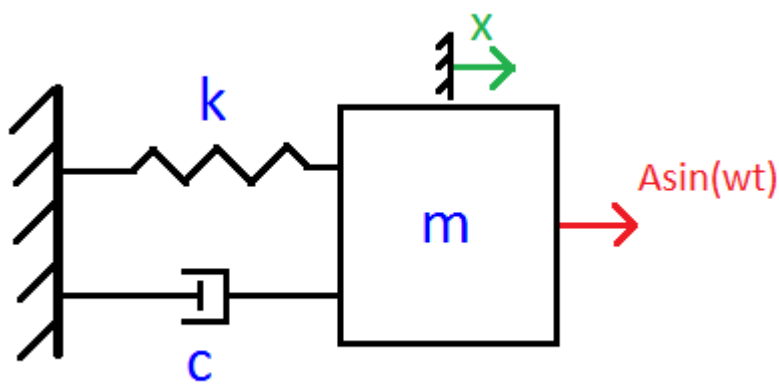

Figure 10. Schematic of Linear Oscillator Model

The equation of motion for this system is

$$m\ddot{x} + c\dot{x} + kx = A\sin(\omega t).$$

This equation can be re-written in the general form

$$\ddot{y} + 2\zeta\omega_n\dot{y} + \omega_n^2 y = \omega_n^2 \sin(\omega t),$$

where

$$y = \frac{x}{x_0}, \quad x_0 = \frac{A}{k}, \quad \omega_n = \sqrt{\frac{k}{m}}, \quad \zeta = \frac{c}{2\sqrt{km}}.$$

Here, ω_n is the natural frequency and ζ is the damping ratio; these are the fitted parameters of the linear oscillator model.

An FRF plot of an example linear oscillator is shown in Figure 11. The amplitude plot (as well as the amplitude plots shown in the models explained later) is color-coded for stability, with blue points representing stable responses and red points representing unstable responses. The real and imaginary parts of the eigenvalues that determine stability are also shown. Note that all responses are stable for the linear oscillator.

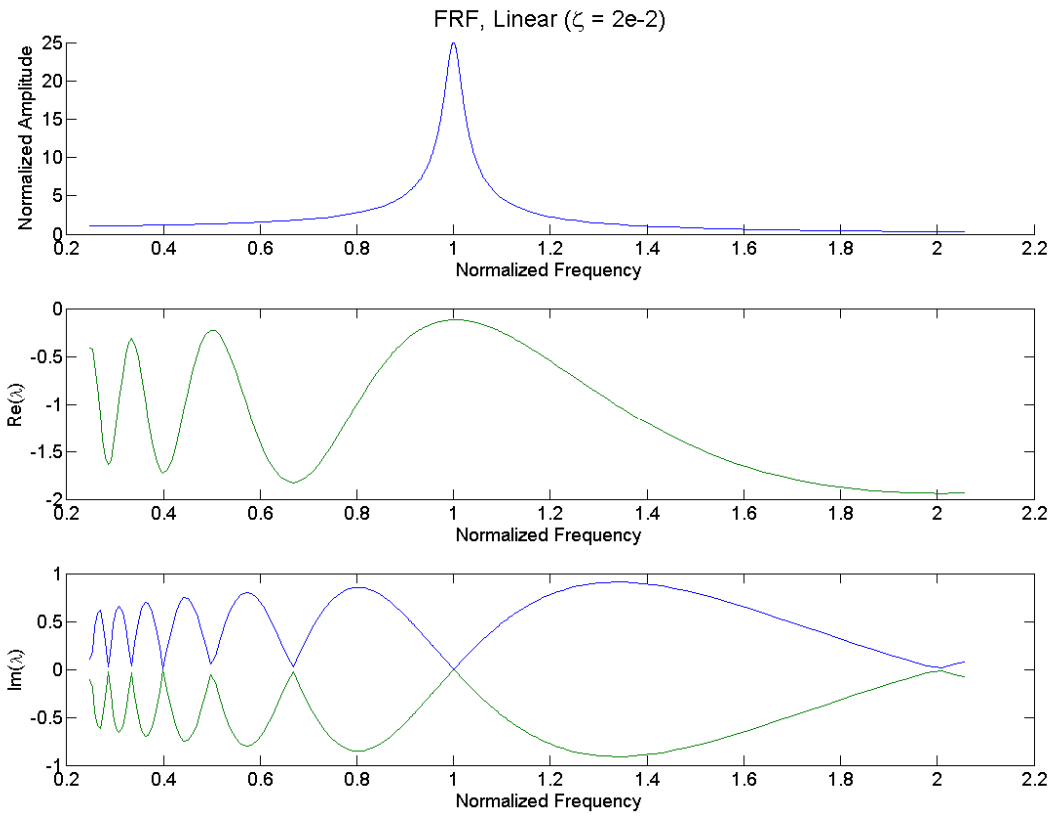

Figure 11: FRF of a linear oscillator in terms of the amplitude, real part of the stability variable (where values greater than 0 indicate unstable responses), and imaginary part of the stability variable.

Note that the FRF in Figure 11 has been normalized to the natural frequency, so only the damping ratio affects the response.

Model and Inverse Model Functions

A plot of the FRF for the normalized position y has a single resonance peak with frequency given by

$$\omega_r \approx \omega_n\sqrt{1-\zeta^2}$$

and amplitude given by

$$y_{r,max} \approx \frac{1}{2\zeta}.$$

These resonance values are the features of interest of this system.

Therefore, the model and inverse model functions for this system are given by

$$M_{Lin}\left(\begin{Bmatrix}\omega_n\\ \zeta\end{Bmatrix}\right)=\begin{Bmatrix}\omega_n\sqrt{1-\zeta^2}\\ \dfrac{1}{2\zeta}\end{Bmatrix}=\begin{Bmatrix}\omega_r\\ y_{r,max}\end{Bmatrix},$$

$$M_{Lin}^{-1}\left(\begin{Bmatrix}\omega_r\\ y_{r,max}\end{Bmatrix}\right)=\begin{Bmatrix}\dfrac{\omega_r}{\sqrt{1-\zeta^2}}\\ \dfrac{1}{2y_{r,max}}\end{Bmatrix}=\begin{Bmatrix}\omega_n\\ \zeta\end{Bmatrix}.$$

Note that in application, the inputs given to M^{-1} are taken from experimental data and the inputs to M are either the outputs of M^{-1} or parameters sampled from a distribution with peaks centered around those outputs. To calculate MFE and MFED, the inputs of M^{-1} are compared to the outputs of M for every combination of data points (as well as every combination of sampled model parameters in the case of MFED).

Summary

A summary of the parameters and functions used for this model in the context of the definitions given in Section 2 is shown below in Table 4.

Table 4. Summary of Linear Oscillator Model

Object(s) from General Definition	***Corresponding Object(s) from Linear Model***
Features of interest, x_i^j (observed) and p_i^j (calculated)	ω_r and $y_{r,max}$
Model parameters, α_n^j (directly from data) and α^η (sampled from PDF)	ω_n and ζ
Model function, $M(\alpha^j)$	M_{Lin}
Inverse model function, $M^{-1}(x^j)$	M_{Lin}^{-1}

APPENDIX B: EQUATIONS FOR DUFFING OSCILLATOR MODEL

A diagram of the system described by the single-DOF Duffing oscillator model is shown in Figure 12, where m, c, k_1 and k_3 are the lumped mass, damping, linear stiffness, and nonlinear stiffness of the system, respectively, and A is the amplitude of a sinusoidal load with angular frequency ω.

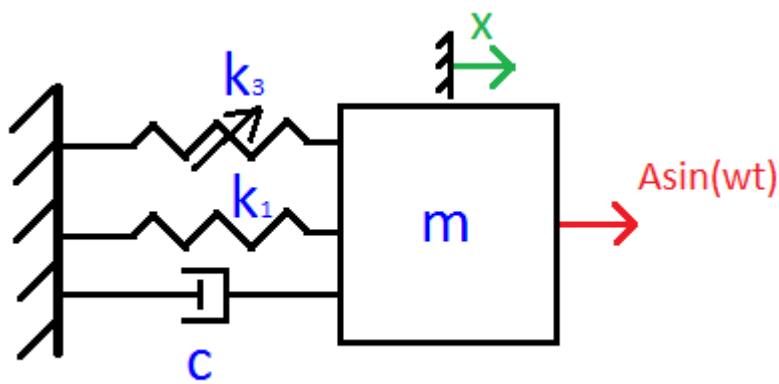

Figure 12. Schematic of Duffing Oscillator Model

The equation of motion for this system is

$$m\ddot{x} + c\dot{x} + k_1 x + k_3 x^3 = A\sin(\omega t)\,.$$

If $k_3 > 0$, the oscillator is said to be hardening because the total stiffness of the system increases as the response amplitude grows large, and the point of maximum response shifts to a higher frequency. Conversely, if $k_3 < 0$, the oscillator is said to be softening because the total stiffness of the system decreases as the response amplitude grows large, resulting in a downward shift in the point of maximum response.

Analytical equations approximating the features of interest of the Duffing model are derived in [18], where the equation of motion is normalized as

$$\ddot{y} + 2\zeta\dot{y} + y + \beta y^3 = \sin(\Omega\tau)\,,$$

where

$$y = \frac{x}{x_0},\quad x_0 = \frac{A}{k_1},\quad \beta = \frac{k_3 x_0^2}{k_1},\quad \omega_n = \sqrt{\frac{k_1}{m}},\quad \zeta = \frac{c}{2\sqrt{mk_1}},\quad \tau = \omega_n t,\quad \Omega = \frac{\omega}{\omega_n}.$$

Here, β is the nonlinearity parameter and ζ is the damping parameter; these are the fitted parameters of the Duffing oscillator model. Note that the notation used in [18] has been altered to maintain consistency with the rest of this report; the nonlinearity parameter α and the forcing function using cos in [18] have been replaced here with β and sin, respectively. Also, it is

important to note that β depends on both the nonlinear spring constant k_3 and the forcing amplitude A.

A plot of the FRF for the normalized position y versus the normalized frequency Ω for a Duffing oscillator has two characteristic frequencies and two corresponding characteristic amplitudes, each representing an apparent instantaneous jump in the response amplitude. These jumps occur because there is a segment of the FRF that is unstable; the responses in this regime can be identified mathematically, but cannot be seen in experiments. The jump-down frequency Ω_d and jump-down amplitude Y_d are the maximum response of the system. The point $(\Omega_d\ , Y_d)$ on the FRF appears in experiments only when the forcing frequency is swept in the direction with the same sign as the nonlinear stiffness parameter k_3 (the positive direction for hardening systems and the negative direction for softening systems). It is followed immediately by a very sharp drop in response amplitude as the unstable regime is skipped over. When the forcing frequency is swept in the opposite direction, the jump-up frequency Ω_u and jump-up amplitude Y_u are identified as the unstable regime is skipped over and the response amplitude undergoes a sharp increase. An FRF of an example Duffing oscillator with color coding for response stability is shown below in Figure 13, along with the real and imaginary eigenvalue parts.

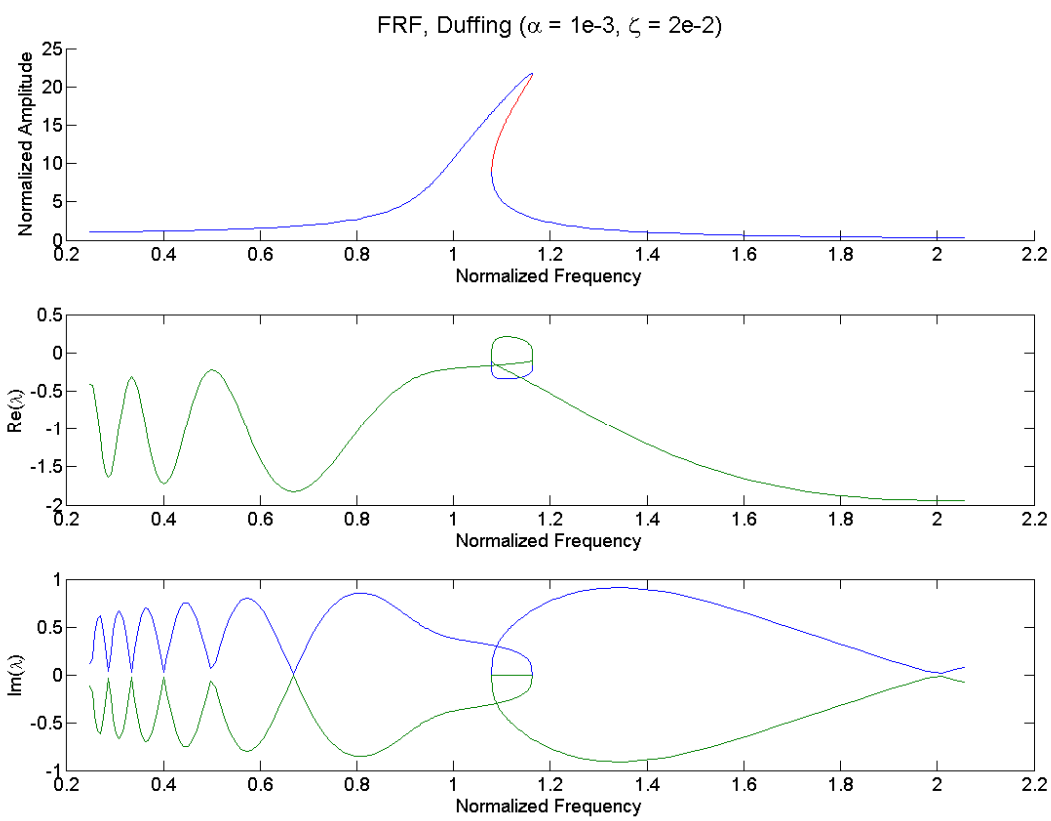

Figure 13: FRF of a linear oscillator in terms of the amplitude, real part of the stability variable (where values greater than 0 indicate unstable responses), and imaginary part of the stability variable. Blue points in the amplitude plot represent stable responses, and red points represent unstable responses.

The features of interest for this system are Ω_d, Y_d, Ω_u, and Y_u. They can be calculated by using analytical approximations derived in [18], or more accurately by plotting the Duffing oscillator FRF for given values of β and ζ. The latter method uses a numerical continuation algorithm to generate an FRF, and the features of interest are found via inspection of the plot. This method tends to be more accurate than the first, but is much more computationally expensive. Theory and implementation of the numerical continuation process are detailed in Appendix F:. Both methods will be explained in detail in what follows.

Model and Inverse Model Functions

Using Analytical Approximations

As was derived in [18], the equations for the features of interest as functions of the fitted parameters β and ζ are given by

$$\Omega_d \approx \frac{1}{2^{1/2}}\left(1+\left(1+\frac{3\beta}{4\zeta^2}\right)^{1/2}\right)^{1/2},$$

$$Y_d \approx \left(\frac{2}{3\beta}\left(\left(1+\frac{3\beta}{4\zeta^2}\right)^{1/2}-1\right)\right)^{1/2},$$

$$\Omega_u \approx \begin{cases} 1+\frac{1}{2}\left(\frac{3}{2}\right)^{4/3}|\beta|^{1/3}, & \beta > 0 \\ 1-\frac{1}{2}\left(\frac{3}{2}\right)^{4/3}|\beta|^{1/3}, & \beta < 0 \end{cases},$$

$$Y_u \approx \left(\frac{2}{3}\right)^{1/3}\frac{1}{|\beta|^{1/3}}.$$

Therefore, the model function for this system is given by

$$M_{Duff}\left(\begin{Bmatrix}\beta\\ \zeta\end{Bmatrix}\right)=\begin{Bmatrix}\dfrac{1}{2^{1/2}}\left(1+\left(1+\dfrac{3\beta}{4\zeta^2}\right)^{1/2}\right)^{1/2}\\ \left(\dfrac{2}{3\beta}\left(\left(1+\dfrac{3\beta}{4\zeta^2}\right)^{1/2}-1\right)\right)^{1/2}\\ \begin{cases}1+\dfrac{1}{2}\left(\dfrac{3}{2}\right)^{4/3}|\beta|^{1/3}, & \beta>0\\ 1-\dfrac{1}{2}\left(\dfrac{3}{2}\right)^{4/3}|\beta|^{1/3}, & \beta<0\end{cases}\\ \left(\dfrac{2}{3}\right)^{1/3}\dfrac{1}{|\beta|^{1/3}}\end{Bmatrix}=\begin{Bmatrix}\Omega_d\\ Y_d\\ \Omega_u\\ Y_u\end{Bmatrix}.$$

By examining the products $\Omega_d Y_d$ and $\Omega_u Y_u$, it is possible to rearrange the equations for the features of interest to obtain more convenient expressions for the fitted model parameters:

$$|\beta|\approx\begin{cases}\dfrac{2}{3}\left(\Omega_u Y_u-\dfrac{3}{4}\right)^{-3}, & \beta>0\\ \dfrac{2}{3}\left(\Omega_u Y_u+\dfrac{3}{4}\right)^{-3}, & \beta<0\end{cases},$$

$$\zeta\approx\frac{1}{2\Omega_d Y_d}.$$

Using these expressions, the two model parameters can be fitted using contributions from all four features of interest. Therefore, the inverse model function for this system is given by

$$M_{Duff}^{-1}\left(\begin{Bmatrix}\Omega_d\\ Y_d\\ \Omega_u\\ Y_u\end{Bmatrix}\right)=\begin{Bmatrix}\begin{cases}\dfrac{2}{3}\left(\Omega_u Y_u-\dfrac{3}{4}\right)^{-3}, & \beta>0\\ \dfrac{2}{3}\left(\Omega_u Y_u+\dfrac{3}{4}\right)^{-3}, & \beta<0\end{cases}\\ \dfrac{1}{2\Omega_d Y_d}\end{Bmatrix}=\begin{Bmatrix}\beta\\ \zeta\end{Bmatrix}.$$

Using Numerical Continuation

Using continuation, a plot of the FRF of the Duffing system for given values of β and ζ can be generated, and the features of interest can be determined by inspection of the data in the plot.

The model function M_{Duff} is therefore a simple process of plotting the FRF curve and determining which data points correspond to the features of interest.

For the inverse model M_{Duff}^{-1}, an optimization method must be used to generate an FRF with minimal error between the computed features of interest and the observed ones. This may require many continuation runs, which makes the computation time much higher than that of the analytical method. Also, if the static (zero-frequency) response of the system isn't shown in the experimental data, the linear natural frequency ω_n and the mass m must be assumed so that the data may be normalized according to the method described above. In that case, ω_n and m may need to be optimized as well.

Summary

A summary of the parameters and functions used for the Duffing Oscillator model in the context of the definitions given in Section 2 is shown below in Table 5.

Table 5. Summary of Duffing Oscillator Model

Object(s) from General Definition	***Corresponding Object(s) from Duffing Model***
Features of interest, x_i^j (observed) and p_i^j (calculated)	Ω_d, Y_d, Ω_u, and Y_u
Model parameters, α_n^j (directly from data) and α^η (sampled from PDF)	β and ζ
Model function, $M(\alpha^j)$	M_{Duff}
Inverse model function, $M^{-1}(x^j)$	M_{Duff}^{-1}

APPENDIX C: DUFFING MODEL WITH AMPLITUDE-AFFECTED DAMPING

Future work may include an MFE analysis for the Duffing model with amplitude-affected damping (DMAAD), with an equation of motion is given as

$$m\ddot{x} + (c_1 + c_2 x^2)\dot{x} + k_1 x + k_3 x^3 = A\sin(\omega t)\,.$$

In addition to the nonlinear stiffness term seen in the Duffing oscillator, the DMAAD has a nonlinear damping term that scales with the square of the position. This means that the overall damping of the system increases with amplitude if $c_2 > 0$ and decreases if $c_2 < 0$.

When normalized, the DMAAD has three fitted parameters: β (nonlinear stiffness parameter), ζ (linear damping parameter), and γ (nonlinear damping parameter). The normalized equation of motion is given by

$$\ddot{y} + (2\zeta + \gamma y^2)\dot{y} + y + \beta y^3 = \sin(\Omega\tau)\,,$$

where

$$y = \frac{x}{x_0},\quad x_0 = \frac{A}{k_1},\quad \beta = \frac{k_3 x_0^2}{k_1},\quad \gamma = \frac{c_2 x_0^2}{k_1},\quad \omega_n = \sqrt{\frac{k_1}{m}},\quad \zeta = \frac{c}{2\sqrt{m k_1}},\quad \tau = \omega_n t,\quad \Omega = \frac{\omega}{\omega_n}.$$

The DMAAD has the same four features of interest as the ordinary Duffing oscillator. However, analytical approximations are not available, so the MFE must be calculated using numerical continuation (as shown in Appendix F:).

An FRF of an example DMAAD that has been color-coded for stability (along with the corresponding real and imaginary eigenvalue parts) is shown below in Figure 14.

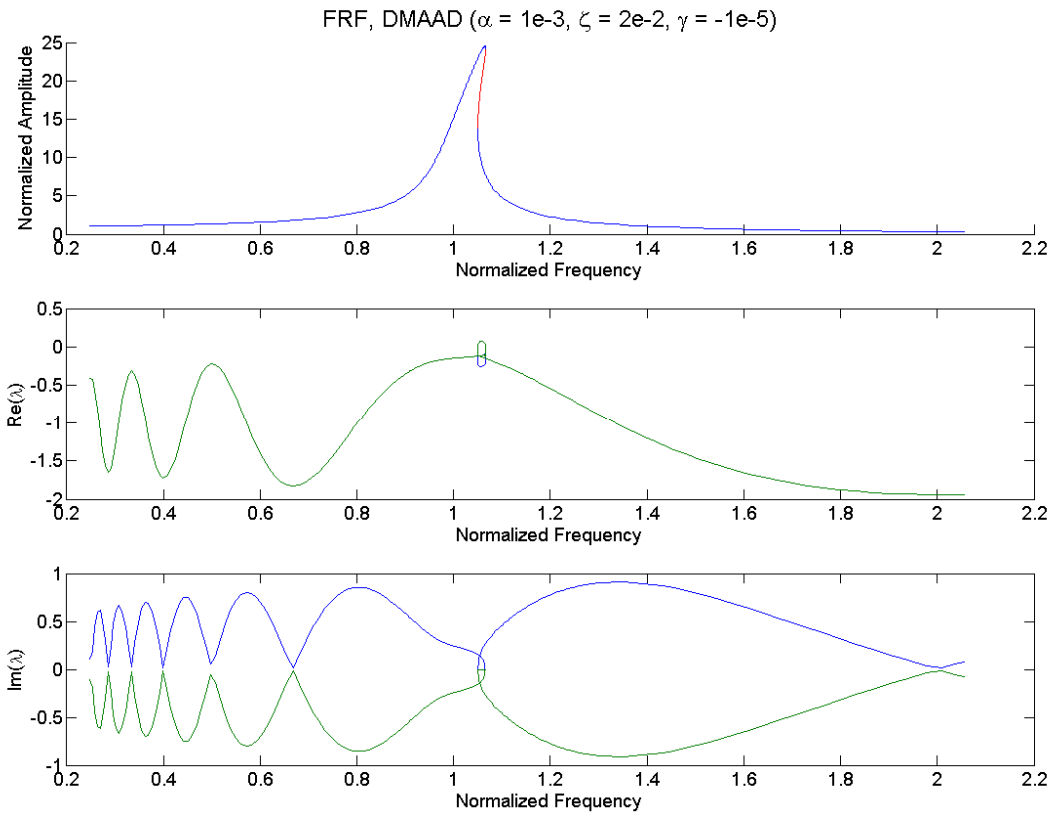

Figure 14. FRF of a Duffing oscillator with amplitude-affected damping in terms of the amplitude, real part of the stability variable (where values greater than 0 indicate unstable responses), and imaginary part of the stability variable. Blue points in the amplitude plot represent stable responses, and red points represent unstable responses.

It should also be noted that if the value of γ is negative and sufficiently large, the overall damping of the system can become negative at large amplitudes. This may result in the appearance of a regime with no stable response in the FRF. This phenomenon is not physical to the tape joint system, but provides some interesting theoretical dynamics nonetheless. An FRF of an example DMAAD with parameters resulting in negative overall damping at large amplitudes is shown below in Figure 15.

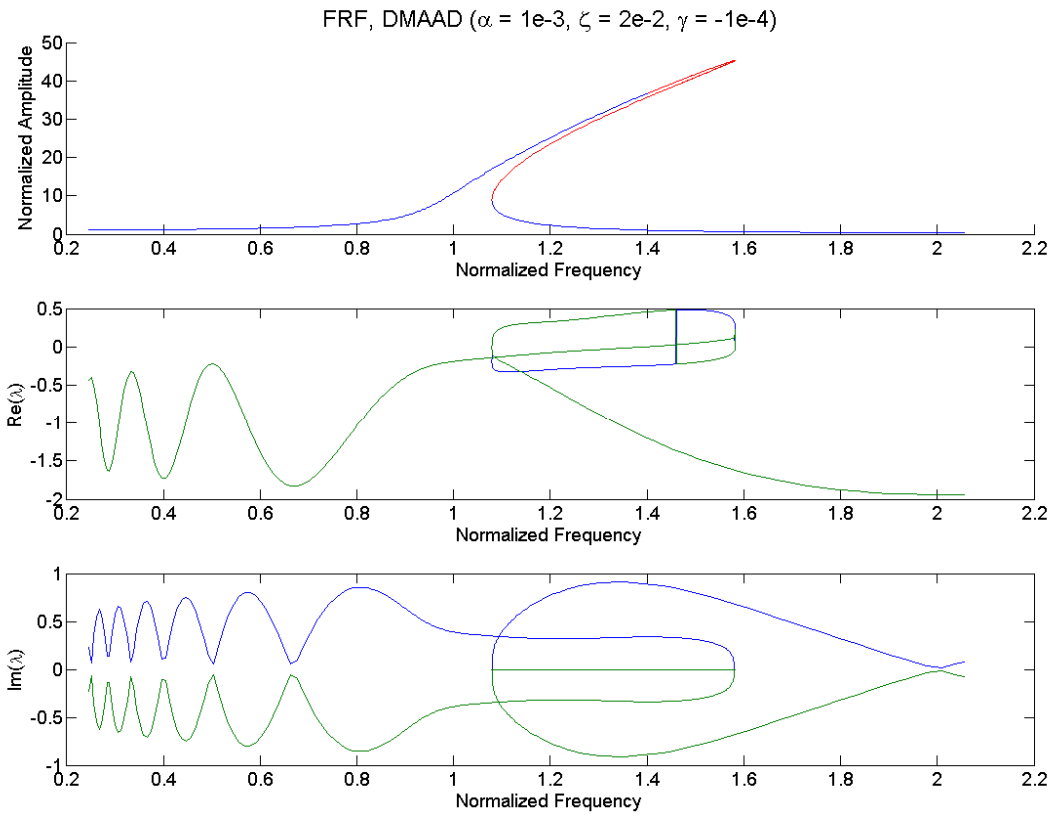

Figure 15. FRF of a DMAAD with negative overall damping with amplitude-affected damping in terms of the amplitude, real part of the stability variable (where values greater than 0 indicate unstable responses), and imaginary part of the stability variable. Blue points in the amplitude plot represent stable responses, and red points represent unstable responses.

APPENDIX D: ONE-WAY COMPLIANT DUFFING OSCILLATOR MODEL

Future work may include an MFE analysis for the one-way compliant Duffing model, whose equation of motion is given by

$$m\ddot{x} + c\dot{x} + k_1 x + k_3(x) * x^3 = A\sin(\omega t)$$

$$k_3(x) = \begin{cases} K_3, & x > 0 \\ 0, & x \leq 0 \end{cases}.$$

When normalized, this equation takes on the same form as that of the ordinary normalized Duffing equation, except that β is replaced by

$$\beta(y) = \begin{cases} \dfrac{K_3 x_0^2}{k1}, & y > 0 \\ 0, & y \leq 0 \end{cases}.$$

The one-way compliant Duffing oscillator has the same four features of interest as the ordinary Duffing oscillator. However, analytical approximations are not available, so the MFE must be calculated using numerical continuation (as shown in Appendix F:).

An FRF of an example one-way compliant Duffing oscillator that has been color-coded for stability (along with the corresponding real and imaginary eigenvalue parts) is shown in Figure 16.

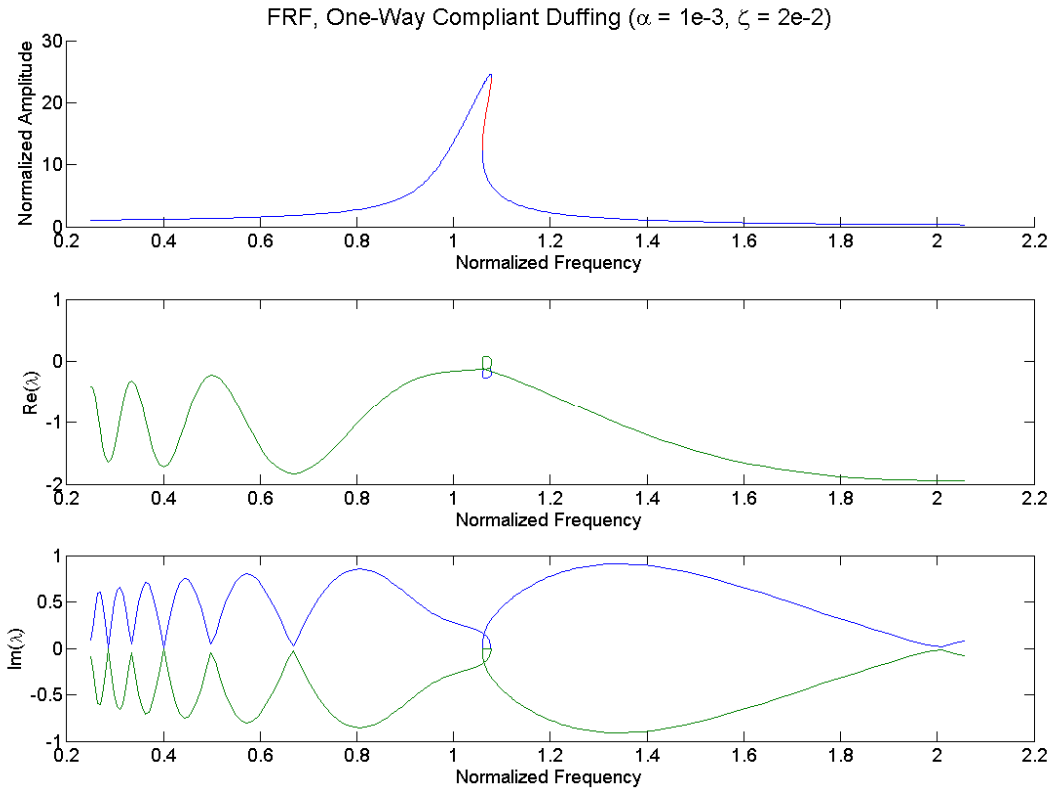

Figure 16. FRF of a one-way compliant duffing oscillator in terms of the amplitude, real part of the stability variable (where values greater than 0 indicate unstable responses), and imaginary part of the stability variable. Blue points in the amplitude plot represent stable responses, and red points represent unstable responses.

APPENDIX E: KERNEL DENSITY ESTIMATION

Kernel density estimation provides a convenient way to estimate the PDF of a distribution for which limited data is available. For example, given a set of n experimental data points x_i, the PDF of the data $f(x)$ can be estimated using a kernel density estimator defined by

$$KDE(x) = \frac{1}{nh}\sum_{i=1}^{n} K\left(\frac{x - x_i}{h}\right),$$

where K (known as the kernel) is a symmetric function satisfying

$$\int_{-\infty}^{\infty} K(y)\, dy = 1$$

and h (known as the bandwidth) is a smoothing parameter. A common kernel (the one used in the tape joint bending application earlier) is the standard normal density function ϕ defined by

$$\phi(y) = \frac{1}{\sqrt{2\pi}} e^{-\frac{1}{2}y^2}.$$

The bandwidth h is crucial in determining the shape of KDE. If h is too small, KDE will have very sharp, distinct peaks centered on the experimental data points. If h is too large, KDE will appear as a single smooth hump with no distinct peaks to identify the experimental data.

After one KDE is calculated for each fitted model parameter, the KDEs can be used to sample a large number of model parameters from distributions that approximate the distributions of the samples taken from experiments. $MFED$ can then be calculated by comparing the model-predicted features of interest for every combination of sampled model parameters with each available experimental data point.

APPENDIX F: NUMERICAL CONTINUATION METHOD

Numerical continuation is a method used to examine the behavior of a system of equations with changes in a free parameter. When given a single solution to a system with a free parameter, a continuation method finds a branch of new solutions corresponding to new values of that parameter. The particular algorithm that was used to compute the Duffing oscillator FRFs mentioned earlier is called pseudo-arclength continuation. Pseudo-arclength continuation is accomplished using the following process:

1. An initial guess is provided.
    - This guess should be close to a solution of the system of equations if possible.

2. A starting solution is calculated.
    - A Newton-Raphson method is used to find a starting solution close to the initial guess.

3. A predictor-corrector method is used to calculate a branch of solutions.
    a. Prediction step:
        - The current solution is used to predict the next solution along the branch. In pseudo-arclength continuation, the prediction is made in a direction tangent to the branch.
    b. Correction step:
        - The predicted solution is used as the initial guess of a Newton-Raphson procedure that should converge on a new solution. In this case, an additional equation is used to constrain the corrections to be orthogonal to the prediction.
        - If a solution is obtained, step 3 is repeated until some stopping criterion is met.
        - If a solution is not found (meaning convergence criteria were not met) within some predetermined number of iterations, the step size of the prediction is reduced, a new prediction is calculated, and the correction step is restarted using the new prediction.

To create the Duffing oscillator FRFs, the pseudo-arclength continuation method is used to compute a branch of periodic orbits with the forcing frequency as the free parameter. The process for finding periodic orbits using continuation (including the steps listed above) is explained in detail in [19]. Using the branch of periodic orbits, vibration amplitudes are calculated for each frequency. These amplitudes are plotted as a function of frequency to obtain the FRFs. From each FRF, the features of interest of the Duffing model are obtained. An example FRF is shown in Figure 17.

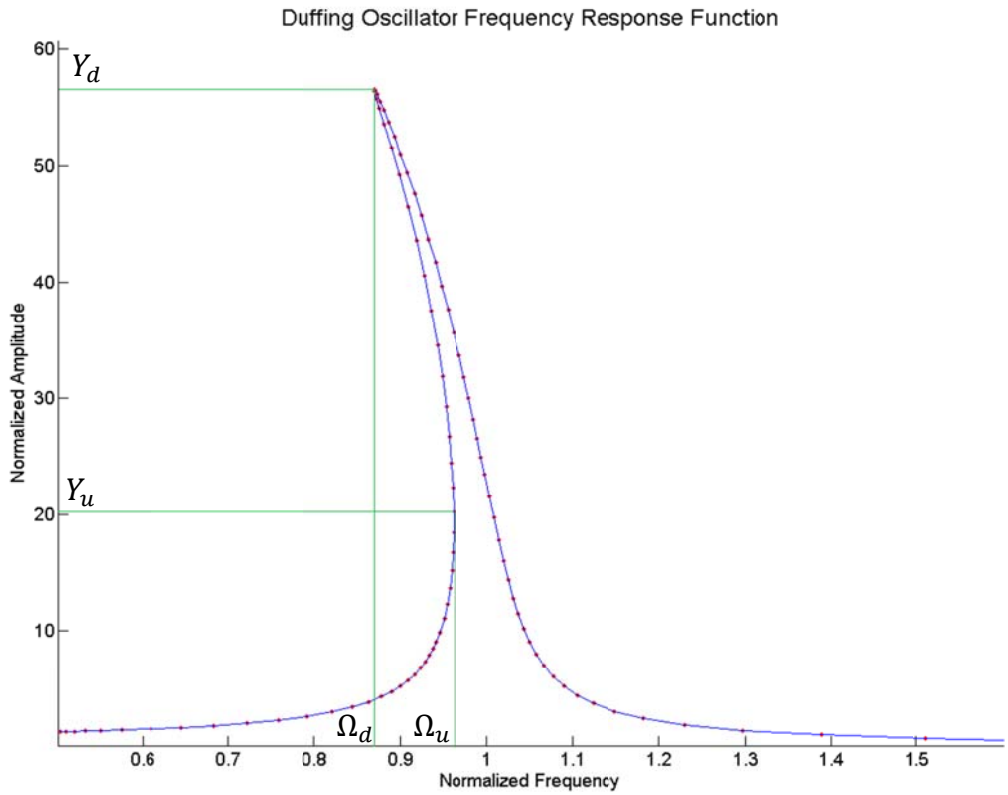

Figure 17. Example of Duffing Oscillator FRF with Features of Interest

REFERENCES

[1] H. Akaike, "A New Look at the Statistical Model Identification," *IEEE Transactions on Automatic Control,* vol. 19, no. 6, pp. 716-723, 1974.

[2] E. T. Jaynes, "Information Theory and Statistical Mechanics," *The Physical Review,* vol. 106, pp. 620-630, 1957.

[3] S. Y. Park and A. K. Bera, "Maximum Entropy Autoregressive Conditional Heteroskedasticity Model," *Journal of Econometrics,* vol. 150, pp. 219-230, 2009.

[4] J. R. Hamilton and R. G. Hills, "Relation of Validation Experiments to Applications: A Nonlinear Approach," *Numerical Heat Transfer, Part B,* vol. 57, pp. 373-395, 2010.

[5] D. J. Segalman, M. R. Brake, L. A. Bergman, A. F. Vakakis and K. Willner, "Epistemic and Aleatoric Uncertainty in Modeling," in *ASME 2013 International Design Engineering Technical Conference*, Portland, OR, 2013.

[6] H. Bozdogan, "Model Selection and Akaike's Information Criterion (AIC): The General Theory and its Analytical Extensions," *Psychometrika,* vol. 52, pp. 345-370, 1987.

[7] H. Bozdogan, "Akaike's Information Criterion and Recent Developments in Information Complexity," *Journal of Mathematical Psychology,* vol. 44, pp. 62-91, 2000.

[8] I. J. Myung, "The Importance of Complexity in Model Selection," *Journal of Mathematical Psychology,* vol. 44, pp. 190-204, 2000.

[9] T. Haag, S. C. Gonzalez and M. Hanns, "Model Validation and Selection Based on Inverse Fuzzy Arithmetic," *Mechanical Systems and Signal Processing,* vol. 32, pp. 116-134, 2012.

[10] W. Zucchini, "An Introduction to Model Selection," *Journal of Mathematical Psychology,* vol. 44, pp. 41-61, 2000.

[11] D. Xiu, J. Jakeman and M. Eldred, "Numerical Approach for Quantification of Epistemic Uncertainty," *Journal of Computational Physics,* vol. 229, pp. 4648-4663, 2010.

[12] K. Chowdhary and P. Dupuis, "Distinguishing and Integrating Aleatoric and Epistemic Variation in Uncertainty Quantification," *ESAIM: Mathematical Modelling and Numerical Analysis,* vol. 47, pp. 635-662, 2013.

[13] C. Soize, "Generalized Probabilistic Approach of Uncertainties in Computational Dynamics Using Random Matrices and Polynomial Chaos Decompositions," *International Journal for Numerical Methods in Engineering,* vol. 81, pp. 939-970, 2010.

[14] K. J. Astrom and P. Eykoff, "System Identification - A Survey," *Automatica,* vol. 7, pp. 123-162, 1971.

[15] W. Gersch, N. N. Nielsen and H. Akaike, "Maximum Likelihood Estimation of Structural Parameters from Random Vibration Data," *Journal of Sound and Vibration,* vol. 31, pp. 295-308, 1973.

[16] W. Gersch, "On the Achievable Accuracy of Structural System Parameter Estimates," *Journal of Sound and Vibration,* vol. 34, pp. 63-79, 1974.

[17] D. J. Segalman and M. J. Starr, "On the Nonlinear Dynamics and Quasi-Statics of Tape Joined Structures," *SAND2012-6527,* 2012.

[18] M. J. Brennan, I. Kovacic, A. Carrella and T. P. Waters, "On the jump-up and jump-down

frequencies of the Duffing oscillator," *Journal of Sound and Vibration*, vol. 318, pp. 1250-1261, 2008.

[19] M. W. Sracic and M. S. Allen, "Numerical Continuation of Periodic Orbits for Harmonically Forced Nonlinear Systems," in *Civil Engineering Topics, Volume 4, Conference Proceedings of the Society for Experimental Mechanics*, 2011.

DISTRIBUTION

1	Sam Wallen University of Washington Department of Mechanical Engineering Seattle, WA 98195		(electronic copy)
1	MS0346	Michael J. Starr	1526 (electronic copy)
1	MS0346	Diane E. Peebles	1526 (electronic copy)
1	MS0372	Chi S. Lo	1524 (electronic copy)
1	MS0557	Charles D. Croessmann	1520 (electronic copy)
1	MS0828	Michael Ross	1523 (electronic copy)
1	MS1070	Matthew R. Brake	1526 (electronic copy)
1	MS9042	Michael L. Chiesa	8259 (electronic copy)
1	MS9042	Daniel J. Segalman	8259 (electronic copy)
1	MS0899	Technical Library	9536 (electronic copy)

Sandia National Laboratories